doi:10.3963/j.issn.1001-487X.2025.01.015

不锈钢06Cr18Ni11Ti与铸钢20Mn的爆炸焊接研究*

朱桂春[1,2],刘中枢[1,2],梁国峰[1,2],黄佳雯[1,2],周大鹏[3],陈 翔[1,2]
(1.江汉大学 省部共建精细爆破国家重点实验室,武汉 430056;2.湖北(武汉)爆炸与爆破技术研究院,武汉 430056;
3.中煤科工集团 淮北爆破技术研究院有限公司,淮北 235000)

摘 要: 不锈钢06Cr18Ni11Ti与铸钢20Mn爆炸焊接复合板可用于高寒地区桥梁建造,为探究不锈钢06Cr18Ni11Ti与铸钢20Mn其焊接界面特征,使用两组不同焊接参数焊接不锈钢06Cr18Ni11Ti与铸钢20Mn。通过光学显微镜和扫描电镜分析焊接界面形态;对样品进行拉伸、弯曲试验以及硬度测试;利用扫描电镜对焊接材料的断口形貌进行分析。结果表明:在界面形态分析中,间隙10 mm的样品熔化层厚度大于间隙4 mm的样品熔化层。界面波纹越大,熔化层越厚。腐蚀铸钢20Mn一侧均观察到焊接界面富集奥氏体,间隙为4 mm的样品未观察到明显孪晶,间隙为10 mm的样品中观察到孪晶。拉伸试验结果表明:界面结合强度大于20Mn强度,间隙4 mm和间隙10 mm的样品均呈韧性断裂。在90°弯曲试验中,焊接界面均未出现分层和裂纹,表现出优异的抗弯性能。在硬度测试中,不锈钢06Cr18Ni11Ti和铸钢20Mn经过爆炸焊接后硬度分别大于各自的原材料硬度,越靠近焊接界面,硬度有着显著的提升,20Mn对加工硬化更加敏感,硬化效果就更加明显。在断口形貌分析中,间隙4 mm和间隙10 mm的样品断口均呈河流状。

关键词: 爆炸焊接;界面形态分析;力学性能测试;晶粒腐蚀;断口分析;孪晶
中图分类号: TG456.6 **文献标识码:** A **文章编号:** 1001-487X(2025)01-0125-08

Study of Explosive Welding Stainless of Steel 06Cr18Ni11Ti/Cast Steel 20Mn

ZHU Gui-chun[1,2], *LIU Zhong-shu*[1,2], *LIANG Guo-feng*[1,2], *HUANG Jia-wen*[1,2], *ZHOU Da-peng*[3], *CHEN Xiang*[1,2]
(1. State Key Laboratory of Fine Blasting, Jianghan University, Wuhan 430056, China;
2. Hubei (Wuhan) Institute of Explosive and Blasting Technology, Wuhan 430056, China;
3. CCTEG Huaibei Blasting Technology Research Institute Co., Ltd., Huaibei 235000, China)

Abstract: Stainless steel 06Cr18Ni11Ti and cast steel 20Mn explosive welding composite plates can be used to build bridges in high alpine areas. Two groups of different welding parameters were used to investigate the weld interface characteristics of stainless steel 06Cr18Ni11Ti and cast steel 20Mn. The explosive thickness was 30 mm, the detonation velocity was 2300 m/s, and the stand-off distances were 4 mm and 10 mm, respectively. The morphology of

收稿日期(Date of reception): 2024-06-21 **网络首发日期(Published online):** 2024-08-23
作者简介: 朱桂春(2000-),男,安徽省马鞍山市,在读硕士研究生,从事爆炸加工方向的研究,(E-mail)z18225551577@163.com。
通讯作者: 陈 翔(1990-),男,安徽省淮南市,博士、副教授,从事爆炸与冲击动力学效应、爆炸加工理论及应用方向的研究,(E-mail)chenxiang@jhun.edu.cn。
基金项目: 国家自然科学基金(12302436);安徽省重点研究与开发计划项目(2022a05020021);中煤科工集团重庆研究院自立科研开发项目(2023YBXM58)
About the author: ZHU Gui-chun(2000-), male, born in Maanshan city, Anhui province, master candidate, mainly engaged in explosive technology, (E-mail)z18225551577@163.com.
Corresponding author: CHEN Xiang(1990-), male, born in Huainan city, Anhui province, Ph. D, associate professor, mainly engaged in explosion and impact dynamics effects, explosion processing theory and applications, (E-mail)chenxiang@jhun.edu.cn.
Fund Programs: National Natural Science Foundation of China(12302436), Anhui Province Key Research and Development Program Project(2022a05020021), Self-supporting Scientific Research and Development Project of Chongqing Research Institute of China Coal Science and Industry Group(2023YBXM58)

the weld interface was studied using an optical microscope and scanning electron microscope, and the samples were submitted to tensile and flexural testing and hardness tests. Furthermore, the fracture morphology of the weld material was studied using a scanning electron microscope. In the interfacial morphology examination, the sample with a 10 mm stand-off distance had a thicker melting layer than the sample with a 4 mm stand-off distance. The melting layer thickens as the contact corrugation increases. Corrosion was observed on the cast steel 20Mn side of the weld interface enriched with austenite. The 4 mm stand-off samples did not exhibit apparent twins, whereas the 10 mm ones did. The 10 mm stand-off samples had higher interfacial deposition energy and strain rate, making twins more likely to occur. Tensile test findings indicated that all fracture separations occurred on the cast steel's 20Mn side. The shear strength of sample 1 ranged from 383.6 to 394.1 MPa, while that of sample 2 ranged from 394.3 to 408.4 MPa, showing binding strength across the interface greater than that of 20Mn. Both 10mm and 4 mm stand-off samples exhibited ductile fracture. In the 90 bending test, the welded interface shows no delamination or cracks, indicating outstanding bending performance. The hardness test results indicate that the hardness of cast steel 20Mn and stainless steel 06Cr18Ni11Ti after explosive welding are higher than that of the corresponding raw materials. Approaching the weld interface, the hardness increases noticeably. The maximum hardness for samples with a 4 mm stand-off is 413.2 HV, while for samples with a 10 mm stand-off, it is 407.9 HV. Work hardening is more pronounced on the 20Mn side of the sample with a 10 mm stand-off. The effect of hardening is much more noticeable. The fractures of the samples with 4 mm and 10 mm stand-offs display a river-like form in the fracture morphology study.

Key words: explosive welding; interface morphology analysis; mechanical property testing; grain corrosion; fracture analysis; twins

1 背景介绍

06Cr18Ni11Ti 是一种奥氏体不锈钢，其因优异的耐腐蚀性、成形性和焊接性而闻名，同时具备良好的机械性能[1]。06Cr18Ni11Ti 广泛应用于化工设备、食品加工、医疗器械、建筑装饰等领域。铸钢 20Mn 是一种常用的低合金铸钢材料，锰含量较高，具有良好的机械性能[2]，通常用于制造承受冲击和磨损的部件[3]。其主要应用在矿山机械、汽车工业、建筑行业和农业机械等领域。大面积 06Cr18Ni11Ti 与 20Mn 复合板可用于高寒地区桥梁建造，由于铸钢 20Mn，焊接性能一般，常规焊接方法焊接的 06Cr18Ni11Ti 与 20Mn 复合板只靠周围的焊缝连接，在焊缝处易发生复合板与基材脱离的问题。

爆炸焊接作为一种高速冲击焊接技术[4-6]，利用由爆炸产生的冲击加载效应，使待焊接的金属材料间产生高速斜碰撞，来实现同种或异种金属间的结合。这种工艺具有材料兼容性好、无需外部热源、焊接速度快、接头质量高等优点，使其在工业领域中得到广泛应用。爆炸焊接 06Cr18Ni11Ti 与 20Mn 复合板服役寿命长，避免后期的修补，但由于铸钢 20Mn 材料在制造过程中原有的缺陷（如孔洞），在爆炸焊接过程可能诱发产生裂纹[7,8]。为探究 06Cr18Ni11Ti 与 20Mn 爆炸焊接界面的微观结构和力学性能，利用光学电子显微镜和扫描电子显微镜分析爆炸焊接界面微观组织分布。通过拉伸、弯曲试验评估爆炸焊接样品的拉伸性能和抗弯性能，并利用维氏硬度计对样品界面附近硬度分布情况进行检测。

2 材料与方法

采用 06Cr18Ni11Ti 不锈钢和 20Mn 铸钢进行实验，06Cr18Ni11Ti 不锈钢尺寸为 200 mm × 100 mm × 4 mm（长 × 宽 × 高），20Mn 铸钢尺寸为 200 mm × 100 mm × 100 mm（长 × 宽 × 高）。

图 1 为爆炸焊接示意图，爆炸焊接前对 06Cr18Ni11Ti 不锈钢和 20Mn 铸钢的待焊接面打磨抛光，飞板与基板平行放置，将基板放置于砧座上，炸药平铺于飞板顶部的炸药盒内，雷管置于飞板短边侧中部[9]。β 为飞板与基板的碰撞角，间隙是飞板与基板之间的距离。实验中使用的炸药为粉状乳化炸药 + 添加物，密度约为 800 kg/m^3，爆速为 2300 m/s，炸药厚度为 30 mm，实验前通过计算，确定药量。且通过实验结果可以看出焊接界面呈现平直状和微波状，说明药量选择在合理范围内，具体爆炸焊接参数见表 1。

实验中，飞板速度（V_p）和碰撞角（β）是计算爆炸焊接参数的重要因素。这种关系可以用下面的公式表示[10]

$$V_p = 2V_D \sin\frac{\beta}{2}$$

式中，V_D 为炸药的爆速。碰撞角 β 可参考《爆破手册》第 828 页的公式计算[11]。

K 为炸药的多方指数。对于常用的铵油炸药 K 值，可以根据炸药的爆速 D（m/s）简单估算[11]

$$K = \sqrt{1 + (D/1067)^2}$$

相关参数及计算结果如表 2。

表 1　爆炸焊接参数

Table 1　Explosive welding parameters

样品	材料厚度/mm	炸药厚度/mm	间隙/mm	焊接结果
1	06Cr18Ni11Ti +20Mn(4 mm +100 mm)	30	4	焊接成功
2	06Cr18Ni11Ti +20Mn(4 mm +100 mm)	30	10	焊接成功

表 2　计算飞板速度 V_P,碰撞角 β

Table 2　Calculated flyer plate velocity V_P, collision angle β

样品	爆速/(m·s^{-1}) V_D	多方指数 K	爆炸比 r	碰撞角 β	碰撞速度/(m·s^{-1}) V_P
1	2300	1.75	0.86	10.70	428.90
2	2300	1.75	0.86	13.00	520.73

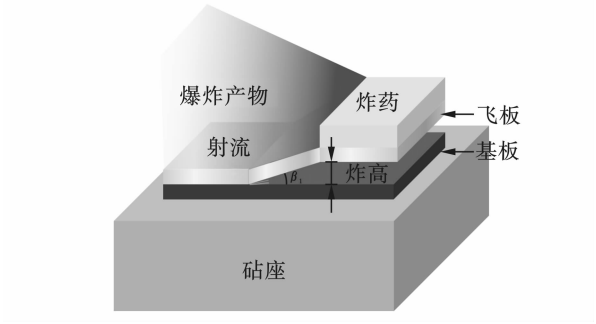

图 1　爆炸焊接装置示意图

Fig. 1　Schematic of the explosive welding device

3　结果与讨论

3.1　界面形态分析

利用光学显微镜对爆炸焊接后样品进行形貌分析,如图 2 所示。样品 1 界面呈平直状,样品 2 界面呈波浪状,间隙越大,碰撞角和碰撞速度越大,可能是由于样品 1 的碰撞角和碰撞速度都小于样品 2[12-19]。由图 2 可知,铸钢 20Mn 区域出现孔洞,铸钢在铸造过程中孔洞的出现是不可避免的,样品 1 和样品 2 的孔洞均没有在冲击载荷下产生裂纹和变形。

对爆炸焊接复合板的 20Mn 区域进行腐蚀。图 3 观察到的白色网状相代表着渗碳体,暗黑色是珠光体,黄色是奥氏体,奥氏体晶粒在焊接界面富集。样品 1 未明显出现孪晶。由图 3(b)可知样品 2 在远离焊接界面处发现孪晶,在参考文献[20]中观察到类似现象。爆炸复合板存在强大的外界作用力,奥氏体晶粒在外力作用力下容易以孪生方式形成孪晶[21,22]。因此,在外界作用力和高温的共同作用下,晶粒内产生孪晶。由于样品 2 焊接界面沉积能量大于样品 1,即样品 2 的应变速率大于样品 1,应变速率的增加更容易诱导孪晶的产生[23]。

图 4 是用扫描电镜观察到的焊接界面图像,更进一步观察界面中熔化层的形貌特征。在爆炸焊接过程中,由于板的撞击,导致焊接界面压力增加,造成金属塑性流动以及金属间的摩擦,使得焊接界面的温度迅速上升,导致焊接界面的局部区域形成熔化层[24]。样品 2 的熔化层相对于样品 1 厚,波状界面明显的地方,熔化层越厚。

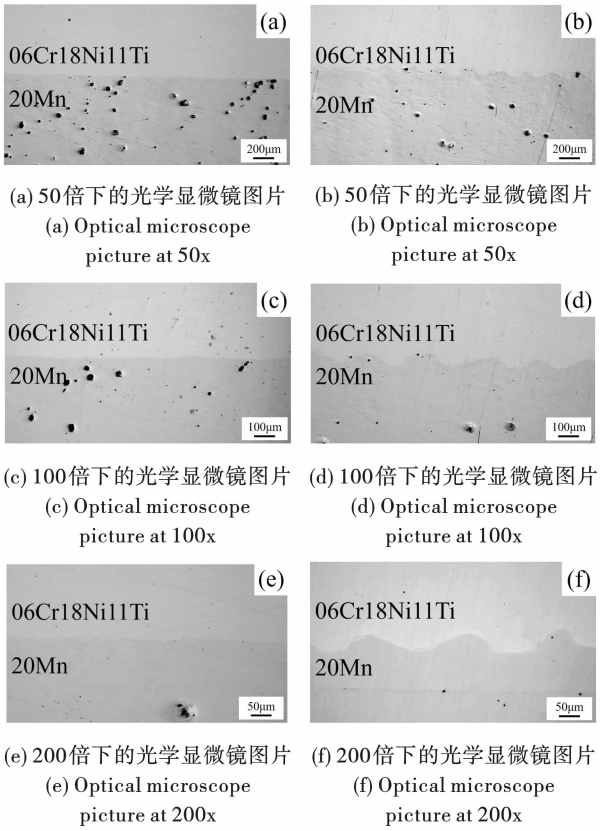

(a) 50倍下的光学显微镜图片 (a) Optical microscope picture at 50x

(b) 50倍下的光学显微镜图片 (b) Optical microscope picture at 50x

(c) 100倍下的光学显微镜图片 (c) Optical microscope picture at 100x

(d) 100倍下的光学显微镜图片 (d) Optical microscope picture at 100x

(e) 200倍下的光学显微镜图片 (e) Optical microscope picture at 200x

(f) 200倍下的光学显微镜图片 (f) Optical microscope picture at 200x

图 2　爆炸焊接的光学显微镜照片

Fig. 2　Optical microscope photographs of explosion welding

图 5 为样品 1 和样品 2 的线扫结果,显示了在界面过渡区域的化学成分变化特性,样品 1 和样品 2 均在熔化层中 Fe 元素的含量急速增加,其中在熔化层中样品 1 和样品 2 的 Cr 元素和 Ni 元素含量减少。

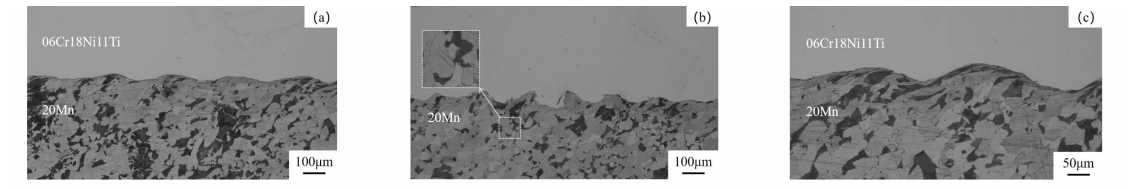

(a) 腐蚀后100倍下的光学显微镜图片
(a) Optical microscope image at 100x after corrosion

(b) 腐蚀后100倍下的光学显微镜图片
(b) Optical microscope image at 100x after corrosion

(c) 腐蚀后200倍下的光学显微镜图片
(c) Optical microscope image at 200x after corrosion

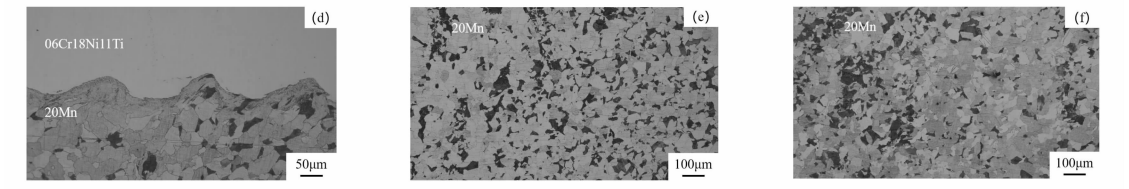

(d) 腐蚀后200倍下的光学显微镜图片
(d) Optical microscope image at 200x after corrosion

(e) 腐蚀后100倍下的光学显微镜图片
(e) Optical microscope image at 100x after corrosion

(f) 腐蚀后100倍下的光学显微镜图片
(f) Optical microscope image at 100x after corrosion

图 3 爆炸焊接后的腐蚀的光学图像

Fig. 3 Optical images of corrosion after blast welding

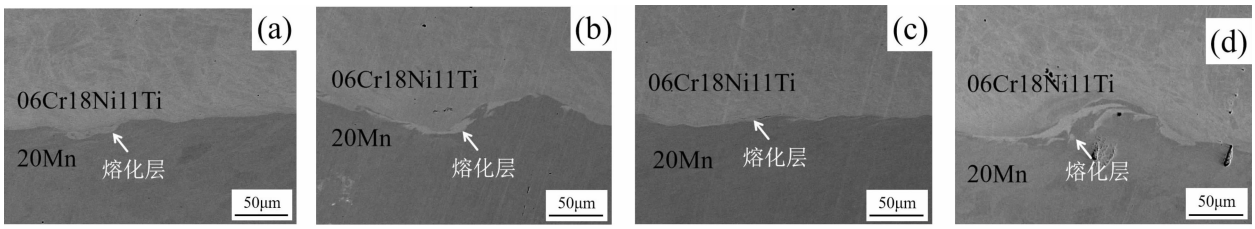

(a) 200倍下的扫描电子显微镜图片
(a) Scanning electron microscope image at 200X

(b) 200倍下的扫描电子显微镜图片
(b) Scanning electron microscope image at 200X

(c) 200倍下的扫描电子显微镜图片
(c) Scanning electron microscope image at 200X

(d) 200倍下的扫描电子显微镜图片
(d) Scanning electron microscope image at 200X

图 4 爆炸焊接界面扫描电子显微镜图像

Fig. 4 Scanning electron microscope images of the explosion welding interface

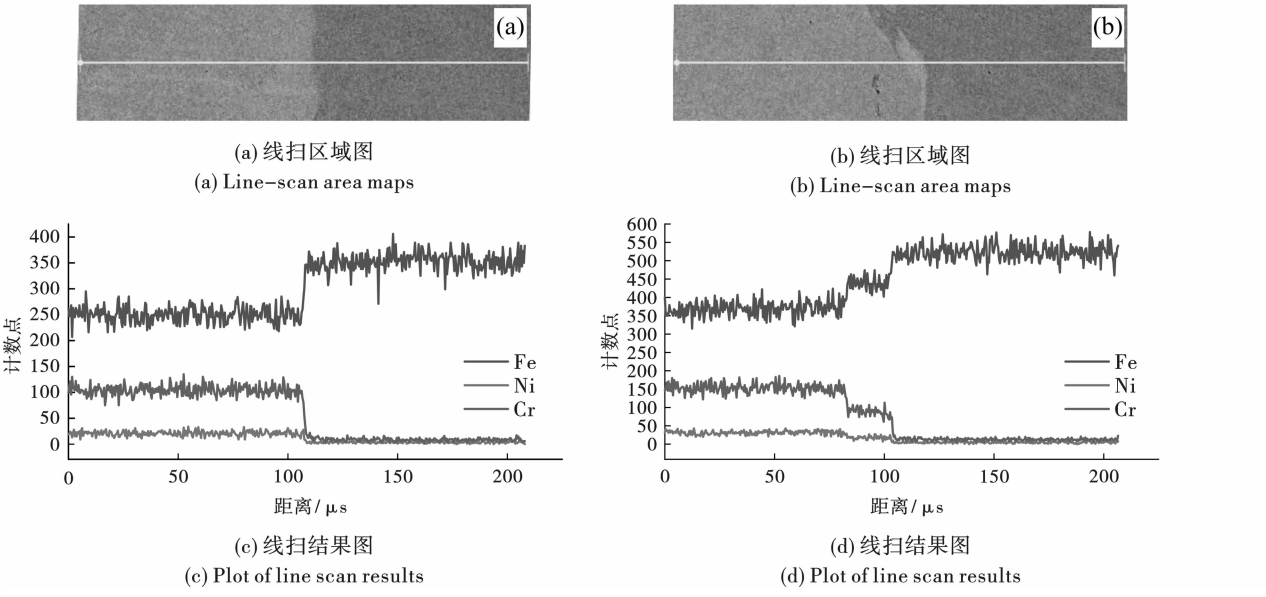

(a) 线扫区域图
(a) Line-scan area maps

(b) 线扫区域图
(b) Line-scan area maps

(c) 线扫结果图
(c) Plot of line scan results

(d) 线扫结果图
(d) Plot of line scan results

图 5 线扫区域及结果图

Fig. 5 Line scan area and results map

3.2　力学性能分析

3.2.1　拉伸剪切试验

对 06Cr18Ni11Ti/20Mn 复合板进行拉伸剪切测试,以评估复合板的焊接结合强度[25,26]。拉剪试件结合面积为 10 mm × 5 mm,试验机的加载速度为 1 mm/min。由表 3 可知样品 1 的抗剪强度为 383.6 ~ 394.1 MPa,样品 2 的抗剪强度为 394.3 ~ 408.4 MPa。从图 6(c)观察到样品断裂均在 20Mn 一侧,说明界面结合强度高于 20Mn。此外,在样品 1 - 2 中还发现 06Cr18Ni11Ti/20Mn 界面出现裂缝,样品 2 - 2 中焊接界面完好。图 6(d)拉伸剪切强度曲线中可以看到断裂过程中有平台期的出现,说明样品呈现韧性断裂。

表 3　拉伸剪切试验结果

Table 3　Tensile shear test results

样品	1 - 1	1 - 2	1 - 3	2 - 1	2 - 2	2 - 3
最大抗剪强度/MPa	394.1	383.6	386.0	408.4	396.3	394.3
裂缝主要位置	20Mn	20Mn	20Mn	20Mn	20Mn	20Mn

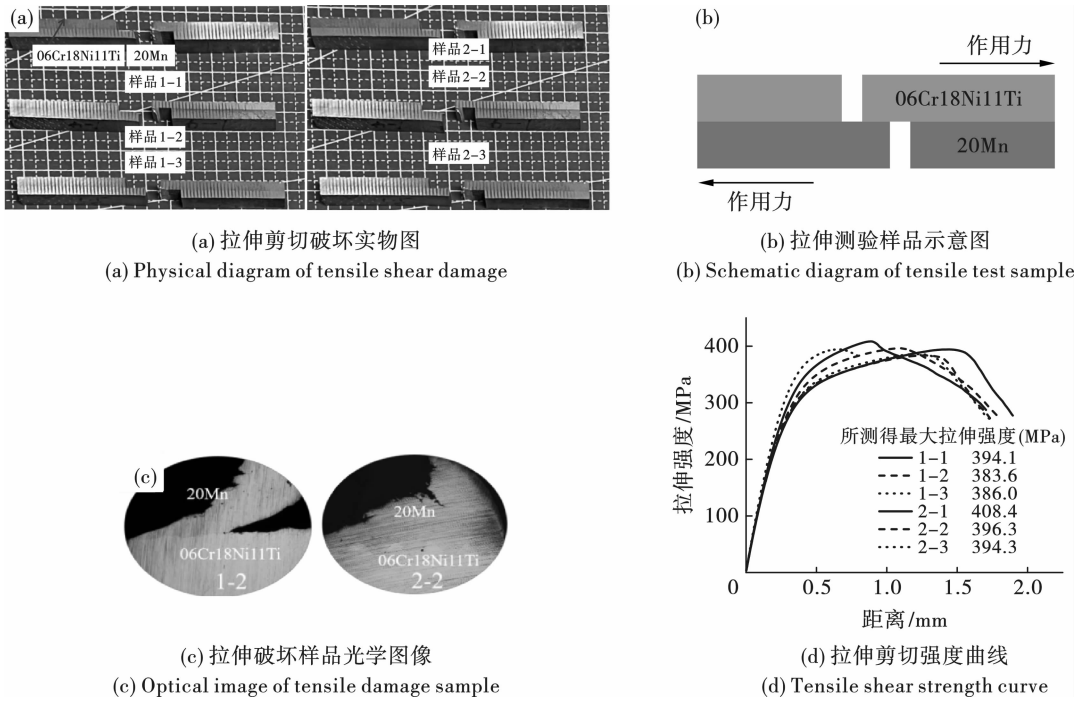

(a) 拉伸剪切破坏实物图
(a) Physical diagram of tensile shear damage

(b) 拉伸测验样品示意图
(b) Schematic diagram of tensile test sample

(c) 拉伸破坏样品光学图像
(c) Optical image of tensile damage sample

(d) 拉伸剪切强度曲线
(d) Tensile shear strength curve

图 6　拉伸剪切测试图

Fig. 6　Tensile shear test chart

不锈钢 06Cr18Ni11Ti/铸钢 20Mn 的断口都发生在 20Mn 一侧,在扫描电镜下观察了 20Mn 的断口形貌。如图 7 所示,样品 1 和样品 2 断口均呈河流状,河流状花样是由于裂纹沿着不同方向的晶面扩展而形成的一种曲折变化的花样,也是呈现解理特征[27-29]。

3.2.2　弯曲试验

弯曲试验也是评估爆炸复合板结合质量的一个重要因素,试验采用三点弯曲试验验证样品是否能够承受 90° 弯曲[30-32]。弯曲试样的样品尺寸为 100 mm × 10 mm × 6 mm(长 × 宽 × 高),试验条件为:加载速率 1 mm/min,加载载荷 10 kN,实验跨距为 50 mm,分别对复合材料的不锈钢 06Cr18Ni11Ti 侧和铸钢 20Mn 侧进行弯曲。由图 9 可知,在对复合材料分别进行不锈钢 06Cr18Ni11Ti 侧弯曲和铸钢 20Mn 侧弯曲时,焊接界面均完好,没有出现明显的分离或开裂现象。由弯曲曲线可以发现铸钢 20Mn 侧弯曲时的弯曲强度大于不锈钢 06Cr18Ni11Ti 侧弯曲,且都能承受 90° 弯曲,说明不锈钢 06Cr18Ni11Ti/铸钢 20Mn 具有良好的塑性,弯曲性能良好。

3.2.3　维氏硬度

界面显微硬度分布如图 10 所示,实验采用 200 N 的负载测量硬度。样品 1 和样品 2 均测试 30 个点,样品 1 和样品 2 中 06Cr18Ni11Ti 侧第一个测点到界面的距离为 40 μm,随后测量间距

200 μm;20Mn 侧第一个测点到界面的距离为 50 μm,随后测量间距为 250 μm。不锈钢 06Cr18Ni11Ti 和铸钢 20Mn 经过爆炸焊接后硬度分别大于各自的原材料硬度,越靠近焊接界面,硬度有着显著的提升,这是由于爆炸焊接引起的加工硬化所导致的硬度提升[33]。样品 2 在 20Mn 一侧最大硬度达到 355 HV,远大于样品 1 在 20Mn 一侧的最大硬度(268 HV)。样品 2 的塑性变形大于样品 1。在图 3 中也观察到样品 2 中 20Mn 一侧的晶粒细化更为显著,且 20Mn 对加工硬化更加敏感,硬化效果就更加明显。

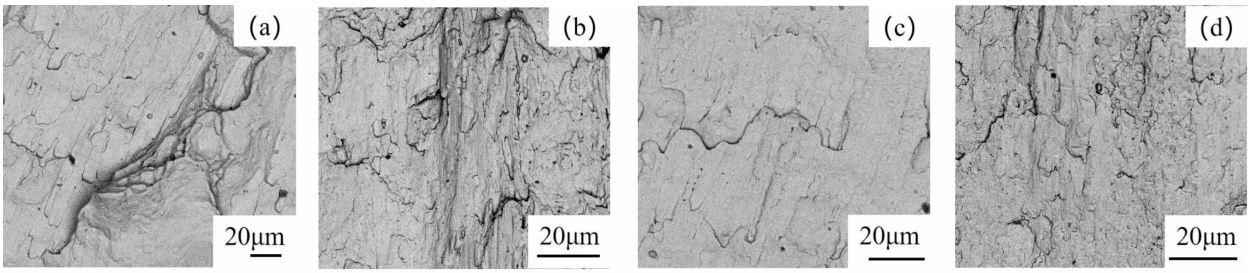

(a) 500倍下的扫描电子显微镜图片 (a) Scanning electron microscope image at 500X

(b) 500倍下的扫描电子显微镜图片 (b) Scanning electron microscope image at 500X

(c) 500倍下的扫描电子显微镜图片 (c) Scanning electron microscope image at 500X

(d) 500倍下的扫描电子显微镜图片 (d) Scanning electron microscope image at 500X

图 7 断口微观形貌图

Fig. 7 Micrograph of the fracture

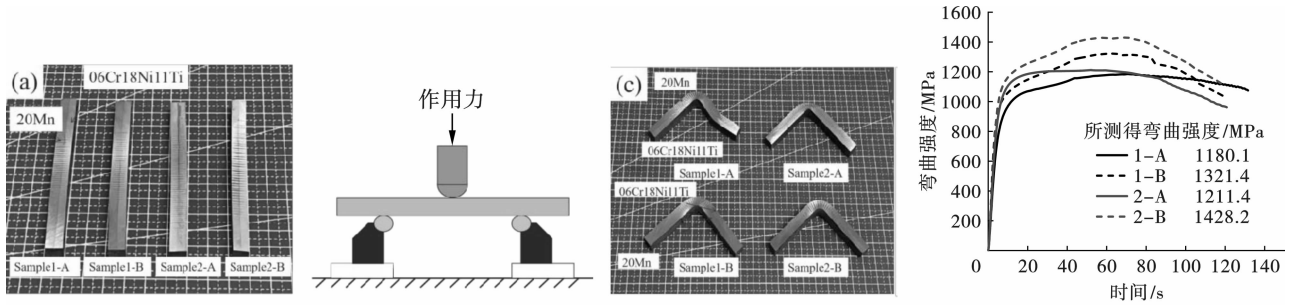

(a) 三点弯曲试验试样实物图 (a) Three-point bending test specimen

(b) 三点弯曲试验试样示意图 (b) Schematic diagram of three-point bending test specimen

(c) 三点弯曲试验实物结果图 (c) Physical results of three-point bending tests

(d) 三点弯曲强度曲线 (d) Three-point bending strength curve

图 8 三点弯曲测试图

Fig. 8 Three-point bending test chart

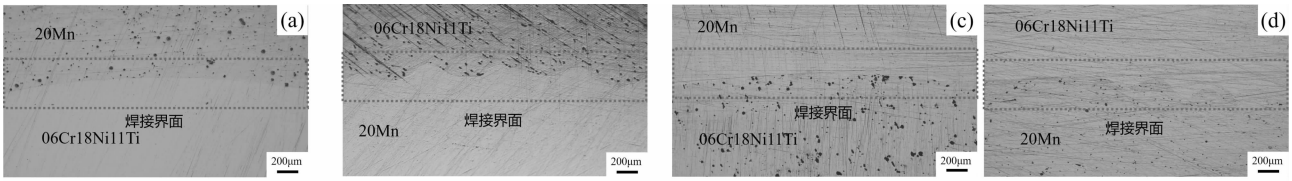

(a) 样品 1-A 在 50 倍下的光学显微镜图片 (a) Optical microscope picture of sample 1-A at 50x

(b) 样品 2-A 在 50 倍下的光学显微镜图片 (b) Optical microscope picture of sample 2-A at 50x

(c) 样品 1-B 在 50 倍下的光学显微镜图片 (c) Optical microscope picture of sample 1-B at 50x

(d) 样品 2-B 在 50 倍下的光学显微镜图片 (d) Optical microscope picture of sample 2-B at 50x

图 9 弯曲试验光学图像

Fig. 9 Optical images of bending test

4 结论

研究通过爆炸焊接技术成功获得了不锈钢 06Cr18Ni11Ti/铸钢 20Mn 合金复合板,分别采取了两组不同的焊接参数进行爆炸焊接,通过对界面组织演变观察、力学性能测试及断口形貌分析得出以下结论:

1)在界面形态分析中,间隙 10 mm 的样品熔化

层厚度大于间隙为 4 mm 的样品熔化层。界面波纹越大,熔化层越厚。铸钢 20Mn 一侧孔洞没有在冲击载荷下产生裂纹。腐蚀铸钢 20Mn 一侧观察到焊接界面富集奥氏体,间隙为 4 mm 的样品未观察到明显孪晶,间隙为 10 mm 的样品中观察到孪晶。由于间隙 10 mm 的所产生的界面沉积能量大于间隙 4 mm 的,即间隙 10 mm 的样品应变速率大于间隙 4 mm 的样品,应变速率的增加更容易诱导孪晶的产生。

2)在拉伸剪切试验中,断裂分离均发生在铸钢 20Mn 侧,界面的结合强度优于母材的强度,对拉伸断口进行分析,断口均呈河流状。样品 1 的抗剪强度为 383.6 ~ 394.1 MPa,样品 2 的抗剪强度为 394.3 ~ 408.4 MPa。在 90°弯曲试验中,均未出现分层与裂纹。在维氏硬度试验中,样品在爆炸焊接后都发生了加工硬化导致界面硬度都高于母材,间隙为 4 mm 的样品最大硬度为 413.2 HV,间隙为 10 mm 的样品最大硬度为 407.9 HV,间隙为 10 mm 的样品 20Mn 一侧对加工硬化更为敏感。

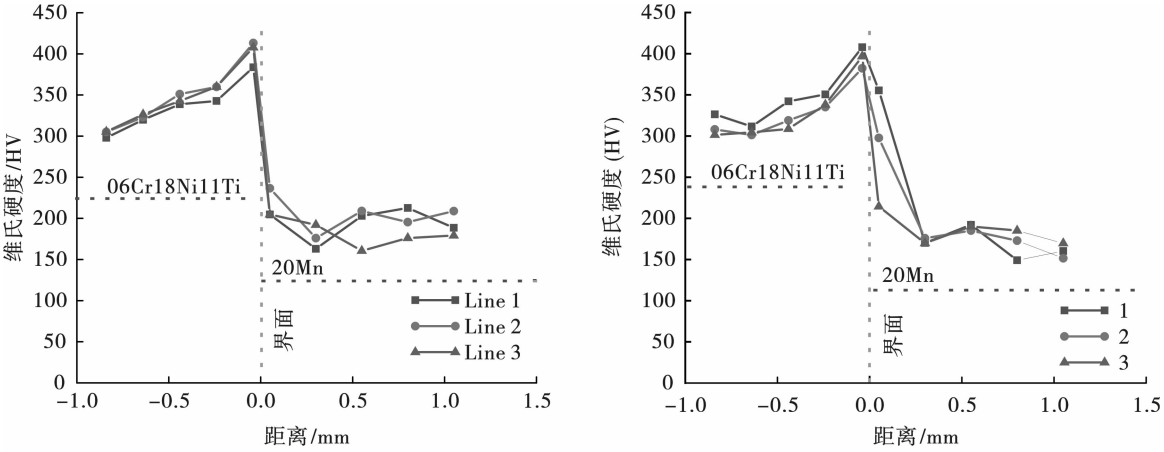

(a) 样品1的界面显微硬度分布
(a) Interfacial microhardness distribution of sample 1

(b) 样品2的界面显微硬度分布
(b) Interfacial microhardness distribution of sample 2

图 10　界面显微硬度分布

Fig. 10　Interface microhardness distribution

参考文献(References)

[1] 梅　荣,任志俊,仇　伟. 06Cr18Ni11Ti 奥氏体不锈钢热变形行为研究[J]. 兵器材料科学与工程,2019,42(6):88-92.

[1] MEI Rong, REN Zhi-jun, QIU Wei. Research on thermal deformation behaviour of 06Cr18Ni11Ti austenitic stainless steel[J]. Weapon Materials Science and Engineering,2019,42(6):88-92. (in Chinese)

[2] 夏少华,陈红圣,曹健峰,等. G20Mn5 铸钢件力学性能研究[J]. 机车车辆工艺,2014(2):9-10,20.

[2] XIA Shao-hua, CHEN Hong-sheng, CAO Jian-feng, et al. Mechanical properties of G20Mn5 cast steel parts[J]. Rolling stock technology, 2014(2): 9-10, 20. (in Chinese)

[3] 康建强,邵光娟,刘宝剑,等. 20MnMoNb 锻板与 0Cr18Ni11Ti 的焊接工艺研究[J]. 设备管理与维修,2020(5):40-42.

[3] KANG Jian-qiang, SHAO Guang-juan, LIU Bao-jian, et al. Research on welding process of 20MnMoNb forging plate with 0Cr18Ni11Ti[J]. Equipment Management and Maintenance,2020(5):40-42. (in Chinese)

[4] 郑远谋. 爆炸焊接和爆炸复合材料[J]. 焊接技术,2007,36(6):1-5.

[4] ZHENG Yuan-mou. Explosive welding and explosive composites[J]. Welding Technology,2007,36(6):1-5. (in Chinese)

[5] 夏鸿博,王少刚,翟伟国,等. 金属爆炸焊接技术研究进展[J]. 热加工工艺,2013,42(5):203-206.

[5] XIA Hong-bo, WANG Shao-gang, ZHAI Wei-guo, et al. Research progress of metal explosion welding technology[J]. Thermal Processing Technology,2013,42(5):203-206. (in Chinese)

[6] WANG Peng, HU Sheng-sun, SHEN Jun-qi, et al. Effects of electrode positive/negative ratio on microstructure and mechanical properties of Mg/Al dissimilar variable polarity cold metal transfer welded joints[J]. Materials Science and Engineering:A,2016,652:127-135.

[7] 郝丁华,吴全银. 16MnR 与 20MnMoNbⅢ异种钢焊接工艺制定及实施[J]. 石油化工应用,2008(2):90-93.

[7] HAO Ding-hua, WU Quan-yin. 16MnR and 20MnMoNb Ⅲ dissimilar steel welding process development and implementation[J]. Petrochemical Applications,2008(2):90-93. (in Chinese)

[8] 徐 然. 530 mm 超厚 20MnMoNb 锻件的窄间隙埋弧焊[J]. 电焊机,2017,47(4):80-84.
[8] XU Ran. Narrow gap submerged arc welding of 530 mm ultra-thick 20MnMoNb forgings[J]. Electric welding machine,2017,47(4):80-84. (in Chinese)
[9] 侯国亭,冯 健,刘献甫,等. 金属复合板节能型爆炸焊接试验研究[J]. 爆破,2023,40(4):161-165,182.
[9] HOU Guo-ting, FENG Jian, LIU Xian-fu, et al. Experimental study on energy-saving explosion welding of metal composite plates[J]. Explosion, 2023, 40(4): 161-165, 182. (in Chinese)
[10] CROSSLAND B. Explosive welding of metals and its application[J]. (No Title),1982.
[11] 汪旭光. 爆破手册[M]. 北京:冶金工业出版社,2010.
[11] WANG Xu-guang Handbook of blasting[M]. Beijing: Metallurgical Industry press,2010.
[12] 赵 昕,宋家良,周大鹏,等. 碳钢-不锈钢水下爆炸焊接的试验研究[J]. 火工品,2023(3):57-60.
[12] ZHAO Xin, SONG Jia-liang, ZHOU Da-peng, et al. Experimental study on underwater explosion welding of carbon steel-stainless steel[J]. Fireworks, 2023(3): 57-60. (in Chinese)
[13] 谢礼宏,段卫东,蒋 培. 爆炸焊接波状界面的 Richtmyer-meshkov 失稳机理[J]. 爆破,2023,40(2):153-158,164.
[13] XIE Li-hong, DUAN Wei-dong, JIANG Pei. Mechanism of Richtmyer-meshkov destabilisation of blast-welded wavy interfaces[J]. Blasting, 2023, 40(2): 153-158, 164. (in Chinese)
[14] ACARER M, GÜLENÇB, FINDIK F. Investigation of explosive welding parameters and their effects on microhardness and shear strength[J]. Materials & design, 2003,24(8):659-664.
[15] WRONKA B. Testing of explosive welding and welded joints. The microstructure of explosive welded joints and their mechanical properties[J]. Journal of materials science,2010,45:3465-3469.
[16] 韩顺昌. 爆炸焊接界面相变与断口组织[M]. 北京:国防工业出版社,2011.
[16] HAN Shun-chan. Interfacial phase transition and fracture organisation in explosion welding[M]. Beijing: National Defence Industry Press,2011. (in Chinese)
[17] XUE Qing, GRAY G T. Development of adiabatic shear bands in annealed 316L stainless steel: Part Ⅱ. TEM studies of the evolution of microstructure during deformation localization[J]. Metallurgical and Materials Transactions A,2006,37:2447-2458.
[18] WANG Min-jing, HU Jia-nian, LI Ke-bin, et al. Study on the relationship between interface morphology and mechanical properties of explosive welded titanium/duplex stainless steel[J]. The International Journal of Advanced Manufacturing Technology,2024:1-20.
[19] HUANG Jia-wen, LIANG Guo-feng, LUO Ning, et al. Study on explosive welding A1060/3D-Printed-SUS316L[J]. Journal of Materials Research and Technology, 2023,27:2508-2523.
[20] 蒋 立. 金属管棒材爆炸焊接界面特性及演化机理研究[D]. 徐州:中国矿业大学,2024.
[20] JIANG Li. Research on the interface characteristics and evolution mechanism of explosion welding of metal tubes and bars[D]. Xuzhou: China University of Mining and Technology,2024. (in Chinese)
[21] PENG Lan, ZHang Jia-quan. Tensile property and microstructure of Fe-22Mn-0.5 C TWIP steel[J]. Materials Science and Engineering: A, 2017, 707: 373-382.
[22] 王 爽. 爆炸复合板焊接接头组织及性能研究[D]. 沈阳:沈阳理工大学,2015.
[22] WANG Shuang. Research on the organisation and properties of welded joints of explosive composite plates[D]. Shenyang: Shenyang University of Science and Technology,2015. (in Chinese)
[23] SHEN Yong-feng, JIA Nan, MISRA R D K, et al. Softening behavior by excessive twinning and adiabatic heating at high strain rate in a Fe - 20Mn - 0.6 C TWIP steel[J]. Acta Materialia,2016,103:229-242.
[24] POTESSER M, SCHÖBERL T, ANTREKOWITSCH H, et al. The Characterization of the Intermetallic Fe-Al Layer of Steel-Aluminium Weldings[C]// Proc of 135th TMS Annual Meeting & Exhibition. 2006:167-176.
[25] ZHANG Heng, JIAO Ke-xin, ZHANG Jia-liang, et al. Microstructure and mechanical properties investigations of copper-steel composite fabricated by explosive welding[J]. Materials Science and Engineering: A, 2018, 731: 278-287.
[26] CHU Qiao-ling, LI Yi, CAO Qi-lu, et al. Microstructure and mechanical properties of Cu/steel dissimilar joints[J]. International Journal of Pressure Vessels and Piping,2022,200:104828.
[27] 姜 超,龙伟民,钟素娟,等. TA1/Q235R 爆炸焊接复合板界面组织及力学性能[J]. 电焊机,2023,53(11):65-70.
[27] JIANG Chao, LONG Wei-min, ZHONG Su-juan, et al. Interfacial organisation and mechanical properties of TA1/Q235R explosion welded composite plates[J]. Electric Welding Machine,2023,53(11):65-70. (in Chinese)

(下转第 182 页)

[10] 彭亚雄,刘广进,苏 莹,等. 基于变分模态分解算法的隧道爆破振动信号光滑降噪模型[J]. 振动与冲击,40(24):173-179.

[10] PENG Ya-xiong, LIU Guang-jin, SU Ying, et al. A smooth denoising model of tunnel blasting vibration signal based on VMD[J]. Journal of Vibration and Shock, 40(24): 173-179. (in Chinese)

[11] 徐振洋,莫宏毅,包 松,等. 基于 VMD-Teager 的露天边坡爆破振动信号能量特征研究[J]. 振动与冲击,2023,42(7):77-88,105.

[11] XU Zhen-yang, MO Hong-yi, BAO Song, et al. Energy characteristics of blast vibration signals of open-pit slope based on VMD-Teager[J]. Journal of Vibration and Shock, 2023, 42(7): 77-88, 105. (in Chinese)

[12] DEHGHANI Mohammad, TROJOVSKY Pavel. Osprey optimization algorithm: A new bio-inspired metaheuristic algorithm for solving engineering optimization problems[J]. Frontiers in Mechanical Engineering, 2023, 8: 1126450. DOI:10.3389/fmech.2022.1126450.

[13] 康怡泽,姚颖康,董润龙,等. 基于 ICEEMDAN-多尺度排列熵的拆除爆破振动信号降噪研究[J]. 振动与冲击,2024,43(13):275-287.

[13] KANG Yi-ze, YAO Ying-kang, DONG Run-long, et al. De-noising of demolition blasting vibration signals based on ICEEMDAN multiscale permutation entropy[J]. Journal of Vibration and Shock, 2024, 43(13): 275-287. (in Chinese)

[14] 孙 远,杨 峰,郑 晶,等. 基于变分模态分解和小波能量熵的微震信号降噪[J]. 矿业科学学报,2019,4(6):469-476.

[14] SUN Yuan, YANG Feng, ZHENG Jing, et al. Research on microseismic signal denoising based on variational mode decomposition and wavelet energy entropy[J]. Journal Mining Science and Technology, 2019, 4(6): 469-476. (in Chinese)

[15] 陈曦明,张军伟,张 冉,等. 一种改进鱼鹰优化算法及其应用[J]. 重庆理工大学学报(自然科学),2024,38(3):122-133.

[15] CHEN Xi-ming, ZHANG Jun-wei, ZHANG Ran, et al. An improved osprey optimization algorithmand its application[J]. Journal of Chongqing University of Technology (Natural Science), 2024, 38(3): 122-133. (in Chinese)

[16] RESHEF D N, RESHEF Y A. FINUCANE H K, et al. Detecting novel associations in large data sets[J]. Science, 2021, 334(6062): 1518-1524.

[17] 彭亚雄. 水下钻孔爆破地震波与水击波协同作用下桥墩动力响应特征研究[D]. 武汉:中国地质大学,2018.

[17] PENG Ya-xiong. Study on the dynamic responses of bridge piers under the synergistic effects of seismic wave and water shock wave induced by the underwater drilling and blasting[D]. Wuhan: China University of Geoscieneces, 2018. (in Chinese)

(上接第 132 页)

[28] 张保奇. 异种金属爆炸焊接结合界面的研究[D]. 大连:大连理工大学,2005.

[28] ZHANG Bao-qi. Study on the bonding interface of dissimilar metal explosion welding[D]. Dalian: Dalian University of Technology, 2005. (in Chinese)

[29] 陶 杰,王咏梅. 复合材料层合板层间破坏及其断口形貌分析[J]. 复合材料学报,1993(4):57-64.

[29] TAO Jie, WANG Yong-mei. Interlaminar damage of composite laminates and morphological analysis of their fracture[J]. Journal of Composite Materials, 1993(4): 57-64. (in Chinese)

[30] PAUL H, CHULIST R, MANIA I. Structural properties of interfacial layers in tantalum to stainless steel clad with copper interlayer produced by explosive welding[J]. Metals, 2020, 10(7): 969.

[31] ZHAO Hui, SHENG Li-yuan. Microstructure and mechanical properties of the Ag/316L composite plate fabricated by explosive welding[J]. Journal of Manufacturing Processes, 2021, 64: 265-275.

[32] 陈 松,李晓杰. 异种金属爆炸焊接的研究与发展[J]. 爆破,2023,40(2):144-152.

[32] CHEN Song, LI Xiao-jie. Research and development of dissimilar metal explosion welding[J]. Blasting, 2023, 40(2): 144-152. (in Chinese)

[33] MENDES R, RIBEIRO J B, LOUREIRO A. Effect of explosive characteristics on the explosive welding of stainless steel to carbon steel in cylindrical configuration[J]. Materials & Design, 2013, 51: 18.